9

Fugitive Dust Emissions from a Coal-, Iron Ore- and Hydrated Alumina Stockpile

Nebojša Topić[1] and Matjaž Žitnik[2]
[1]*Luka Koper, d.d., Koper*
[2]*Jožef Stefan Institute, Ljubljana and*
Faculty of Mathematics and Physics,
University of Ljubljana
Slovenia

1. Introduction

Dust control measures must be implemented in order to reduce the detrimental and harmful effects on material and human resources. According to Mohamed & Bassouni (2006), besides causing additional cleaning of homes and vehicles, fugitive dust can affect visibility and, in severe cases, it can interfere with plant growth by clogging pores and reducing light reception. In addition, dust particles are abrasive to mechanical equipment and damaging to electronic equipment such as computers.

Of the total suspended material, the PM10 fraction (the inhaled dust) is particularly problematic. The US Environmental Protection Agency (US EPA, 1996) reports that a 50 $\mu g/m^3$ increase in the 24 hr average PM10 concentration was statistically significant in increasing mortality rates by 2.5%–8.5% and hospitalization rates due to chronic obstructive pulmonary disease by 6%–25%. It also describes how children can be affected by short-term PM10 exposure by increasing the number of cases of chronic cough, chest illness, and bronchitis (US EPA, 1996). The chronic effects from PM10 depend on the composition of the dust and on the amount of exposure to PM10 over a person's lifetime. A wealth of epidemiological data support the hypothesis that on average, for every 10 $\mu g/m^3$ rise of the total mass concentration of PM10 in the air there is an 1 % increase in cardiovascular mortality on a day-to-day basis (Routledge & Ayers, 2006). In addition to health effects there are other adverse impacts from PM10 exposure. For instance, it is thought that the amount of PM10 contributes to climate change, because the small particles in the atmosphere absorb and reflect the sun's radiation, affecting the cloud physics in the atmosphere (Andrae, 2001).

One of the strong dust emitter sources are large stockpiles of material such as coal and iron ore that are stored and manipulated in the open and exposed to the varying weather conditions. Coal is a mixture of compounds and contains mutagenic and carcinogenic polycyclic aromatic hydrocarbons. Exposure to coal is considered as an important non-cellular and cellular source of reactive oxygen species that can induce DNA damage as shown for wild rodents in an open coal mining area (Leon et al., 2007). In addition, coal is a well known respiratory toxicant and employees who work around coal stockpiles are susceptible to black lung (pneumoconiosis) (Peralba, 1990). With respect to the workers handling the material at above ground facilities,

the risk of suffering a death of a lung cancer or pneumoconiosis for an underground worker is expected to be much higher due to additional presence of radon and more limited means of ventilation (Archer, 1988). Iron ore is often found in a form of hematite, the mineral form of iron (III) oxide (Fe_2O_3). Chronic inhalation of excessive concentrations of iron oxide fumes or dusts may result in development of a benign pneumoconiosis, called siderosis (Nemery, 1990). Inhalation of excessive concentrations of iron oxide may enhance the risk of lung cancer development in workers exposed to pulmonary carcinogens. According to a study by Boyd et al. (1970) who investigated the mortality of 5811 Cumberland iron-ore miners who died between 1948 and 1967, the miners who work underground suffer a lung cancer mortality about 70% higher than "normal". However, besides the carcinogenic effects of iron oxide the risk may be also due to radioactivity in the air of the mines (average radon concentration of 100 pCi/l), since the same study found no evidence of any excess mortality from lung cancer among surface workers. The study of Lawler et al. (1985) of 10403 Minnesota iron ore (hematite) miners found no excesses of lung cancer mortality among either underground or above ground miners. This "no risk" result is different from other studies and, according to some authors can be explained by the apparent absence of significant radon exposure, a strict smoking prohibition underground, an aggressive silicosis control programme, and the absence of underground diesel fuel at the location. Hydrated alumina (Aluminium hydroxide: $Al_2O_3.3H_20$) is known to cause mild irritation to eyes, skin and the upper respiratory tract. It can lead to aggravation of medical conditions such as asthma, chronic lung disease and skin rashes. King et al. (1955) studied the exposure to guinea pigs to alumina and found no harmful effects in lungs after one year.

In a typical open air coal terminal dust arises through activities such as loading, unloading, storage and transport of the millions of tonnes of coal that the terminal handles on average each year. To estimate reliably the quantity and composition of dust emitted by stored material upon different wind conditions, a characterisation of the basic dusting processes is required. This consists in measuring quantity of the material lost and concentration of dust emitted by suitably prepared surface at different local wind velocities as a function of material type, granule size and moisture. Below we report on dust emission measurements of a test unit surface, performed on a wind stream test track set up at the open air terminal (EET) of the Port of Koper. Time dependence of mass loss from the test surface was measured together with concentrations of inhalable particulate matter (PM10) and black carbon (BC) in the vicinity of the test surface for a range of different wind velocities. Threshold wind velocities were measured for four different size fractions of coal and for three different fractions of iron ore stored at the terminal, and for hydrated alumina - a strong dust emitter that is also handled by the port. The same set up was employed to study the suppression of dust emitted by the finest coal fraction and iron ore upon watering of the dry test surface. Although CFD calculations of a large real scale physical configuration are necessary to obtain the final result concerning emissions from the realistic stockpile, the precise measurements of the "dusting" potential generated by the "unit" test surface under different conditions are of significant value.

2. Scientific background

Dusting continues to be an important topic in environmental research. Globally, scientists are studying the induction of dust in order to devise accurate models of dusting as part of

efficient dust mitigation and control measures. A significant corpus of literature now exists concerning fugitive dust emissions, dust erosion, wind erosion, and importantly studies of dusting from stockpiles. The most important of the early studies is considered that of Bagnold (1941), who initiated oriented aeolian research as a result of investigating dune formation. Since Bagnold's initial studies, a number of efforts have been devoted to understanding the erosion mechanisms of wind-blown particles in regards desert expansion (White, 1998; Parsons et al., 2004), farmland erosion (Saxton et al., 2000) and the assessment of coal and mineral dust pollution (Lee & Park, 2002; Gillette, 1977; Cowherd et al., 1988; Chane Kon et al., 2007). Other research has focused on dusting from open coal mining (Chakraborty et al., 2002), dusting from unpaved and paved roads (US EPA 1995; Gillette, 1977; Ferrari, 1986), and dusting from open stockpiles located at ports and power stations (Lee & Park 2002; Nicol & Smitham, 1990; Smitham & Nicol, 1990). Within the port, most loose bulky materials have the potential to generate dust during handling. It can be generated either while the material is being transported to storage, or while the material is in a static storage state like a stockpile. During stockpiling, the coal in the surface layers experiences a range of climatic conditions. Intuitively, one would expect that the factors affecting dusting are the surface area of the coal exposed, the particle size of the coal in the surface layer, the velocity of the prevailing wind, and the effect of moisture in the surface layer.

2.1 Erosion modeling

Today, most research is oriented towards developing accurate wind erosion models (Gillette, 1977). As a result, it is known that fine particle erosion from material stored in open yards is a consequence of the wind acting on the region next to the pile surface. The forces acting on the particles include gravity, pressure and viscosity. The gravity force depends on the diameter of the material and its mass; the forces of pressure and viscosity depend upon the flow field generated around the pile. The sum of these forces, if resolved in the direction of the flow and in a perpendicular direction to it, results in the so-called aerodynamic forces: lift force and drag force, respectively. Bagnold (1941) was one of the first to identify the three modes of particulate transport:

- **Creep:** Large particles that are too heavy to be lifted from the surface by the wind can roll along the surface. This is known as creep or surface creep motion. Creep constitutes between 5% and 25% of the total particle transport during a wind erosion event. As particles roll, they abrade the surface and produce or liberate dust particles. Nonetheless, the amount of dust emitted from this mode of transport is relatively small.
- **Saltation:** Particles that are lifted from the ground by aerodynamic forces, but are too heavy to be dispersed into the atmosphere by the wind turbulence, hop across the surface. This type of motion is referred to as saltation. Saltation is the principal process of wind erosion and accounts for roughly 50% to 80% of the bulk of the total particle transport.
- **Suspension:** this is the transport of fine dust particles that are dispersed into the atmosphere and carried away over large distances. Wind alone usually cannot entrain the fine dust particles directly into suspension. This is due to the strong cohesive forces that bind fine particles together (Shao et al., 1993).

These different transportation mechanisms are important as they act to remove the material from the stockpile test area. The measurements that are reported are designed to investigate the removal of different size fractions of material from a test area. The measurements included: i) the suspension loss i.e., detection of PM10 fraction and, ii) the total removal of particles from the test area (mass loss) with all three transportation mechanisms at different wind speeds. The wind field situation is characterized by both, geometry and wind source strength. To interpret the data and compare the findings from this study with previous ones, which apply to a flat terrain situation without obstacles, it is important to know the flow characteristics around the test area.

2.2 The emission factor according to the US EPA

The study of dust is complicated by the many variables that need to be considered. Therefore, any theoretical/numerical simulation would probably result in the forced assumption of several simplifications (Witt et al., 2002). Alternatively, an empirical valuation covers only a limited range of working conditions; even more, for a given location if the conditions are in flux (Kinsey et al., 2004). In trying to establish a level of airborne dust generated from an open pile, one of the most extended methodologies is the US EPA method (US EPA, 1998), which provides the emission factors and procedures required to estimate total emissions. For stockpiles, the US EPA gives several parameters and inputs for cone and flat top oval configurations (Stunder & Arya, 1988). Emissions from stockpile activities may be estimated using the information from sections 13.2.4 and 13.2.5 of the AP-42 Compilation of Air Pollutant Emission Factors document (US EPA, 1995). The methodology applied in section 13.2.5, Industrial Wind Erosion, requires that the initial wind parameters be established; this being the fastest mile used to convert the values obtained from reference anemometers to friction velocity u^*,

$$u^* = 0.053 \cdot u_{10}^+ \tag{1}$$

The fastest mile of wind at a height of 10 m is denoted by u_{10}^+. This equation only applies to flat piles or those with little penetration into the surface wind layer. The wind speed profile in the surface boundary layer follows the following logarithmic distribution:

$$u(z) = \frac{u^*}{K} \ln \frac{(z - Z)}{z_0}, \qquad z \geq Z \tag{2}$$

where u is the wind speed, z is height above the test surface, z_0 is the roughness height, Z is the zero plane displacement and K=0.4 is von Karman's constant. The friction velocity u^* is a measure of wind shear stress on the erodible surface, as determined from the slope of the logarithmic velocity profile. The roughness height z_0 is a measure of the roughness of the exposed surface. According to EPA methodology the emission factor E_f for surface airborne dust subject to disturbances may be obtained in units of grams per square metre per year ($g/m^2/year$) as follows:

$$E_f = k \sum_{i=1}^{N} P_i S_i \tag{3}$$

where k is the particle size multiplier, N is the number of disturbances per year, P_i is the erosion potential corresponding to the observed fastest mile of wind for the i-th period between disturbances in g/m⁴, and S_i is the pile surface area in m². The particle size multiplier in Eq. (3) varies with aerodynamic particle size and is reported in Table 1.

Particle Size	30 μm	< 15 μm	< 10 μm	< 2.5 μm
Multiplier k	1.0	0.6	0.5	0.2

Table 1. Aerodynamic particle size multipliers in Eq. (3) (After US EPA, 1995).

The erosion potential P for a dry, exposed surface is calculated from

$$\begin{aligned} P &= 58\,(u^* - u_t^*)^2 + 25(u^* - u_t^*), \qquad u^* \geq u_t^*, \\ P &= 0, \quad u^* < u_t^* \end{aligned} \tag{4}$$

where u^*_t is the threshold friction velocity in m/s. Therefore, erosion is affected by particle size distribution and by the frequency of a disturbance; because of the nonlinear form of the erosion, each disturbance must be treated separately. Eq. (1) assumes a typical roughness height of 0.5 cm and height to base ratio not exceeding 0.2. If the pile exceeds this value, it would be necessary to divide the pile area into sub-areas of different degrees of exposure to wind. When working with higher height ratios the following formulas must be employed:

$$u^* = 0.10\,u_s^+ \tag{5}$$

with

$$u_s^+ = \frac{u_s}{u_r} u_{10}^+ \tag{6}$$

US EPA (1995) suggests, for representative cone and oval top flat pile shapes, the ratios of surface wind speed (u_s) versus the approaching wind (u_r) are derived from wind tunnel studies. Hence the total surface of the pile is subdivided into areas of constant u^* where Eqs. (4) – (6) can be used to determine u^*. A convenient methodology therefore exists to generate rough estimates for the gross dust output of the large stock area if the material stored and the asymptotic wind conditions are known. However, the aim of this work is to obtain data, which can yield accurate and detailed estimate of the dust output of a real stockpile, in particular PM10. This study aims to measure the dependence of dust emissions on the wind velocity for coal, iron-ore and hydrated alumina to provide supplemental generic parameters of the corresponding erosion potentials.

2.3 Evaluation of dusting from transport operations

An important information is also how much dust the port produces during the loading of trucks or wagons with truck loaders as well as during the massive unloading of ships. Chakraborty et al., (2002) has developed twelve empirical formulae to calculate the suspended particulate matter emission rate from various opencast coal/mineral mining activities. The measured and calculated values of the emission rate have been compared for each activity and, as reported, they agree to 77.2 – 80.4%. Many of the activities quoted in

Table 10 of their paper are similar to those at the open air terminal but there are additional site-specific assumptions that must be taken into account. For example, the dust emitted during loading of crusted material is different from the case of completely dry and crushed material. It is obvious, when assessing the final dusting situation, such activities can not be neglected. For example, the measurements at the open air terminal in Port of Koper revealed a base level weekly concentration of Fe in the PM10, determined by the sole presence of the stockpile, over which several times larger concentrations are superimposed during short times of intensive unloading activities of the iron-ore (Žitnik et al., 2005). However, the estimation of emission levels generated by different port activities is not in the focus of the present work.

2.4 Wind tunnel studies

In wind tunnel studies particulate emissions from cargo unloading and handling activities are usually not considered, although they can make an important contribution to the total amount of dust emitted. Borrego et al. (2007) made a maquette (1/333) of the port of Leixoes in North Portugal – a scrap metal pile, in order to reduce the particulate emission from the site. They found that while large particles emitted during material handling mostly settled before reaching residential areas, higher daily mean concentrations of PM10 were detected inside nearby houses (200 m away) than at the site (30 m). The proposed technical solutions, the upwind and downwind barrier were tested in a wind tunnel. The use of a smoke and laser sheet allowed the authors to visualize the turbulent structures of the local wind field for wind velocity magnitudes of 2 - 11 m/s. From the scaled down data and using the EPA's compilation (US EPA, 1995), they estimate that about 65% less PM10 is emitted from the top of the pile, mostly due to the reduced wind velocity and redirection of the wind flow for both the upwind porous barrier and downwind container barriers. Unfortunately, the authors do not report the effects in a 1:1 situation, which was realized on account of their findings (with solid windbreaks). In a similar wind tunnel study, Ferreira & Oliveira (2008) make use of an electronic balance with precision 0.05 g, and a model box filled with dusting test material. The authors filled a transparent parallelepiped box (99 x 420 x 145 mm^3) with dry sand with grain diameter of $d \approx 0.5$ mm. In each experiment the test box was filled to form, initially, a flat "free-surface" levelled at a depth of 10 mm below the box surface. An undisturbed wind velocity of 11.4 ± 0.4 m/s was used in all the experiments. The maximum emission rate occurred in the initial stage, when the box was still full but became practically zero after one hour. The maximum mass loss rate per unit surface q can be compared with a flat bed situation for which Bagnold (1941) suggested the following formula

$$q = C\sqrt{d/D}\,\frac{\rho}{g}(u_t^*)^3 \tag{7}$$

where C=1.5 m^{-1} for a uniform sand, D is a grain diameter of the standard 0.25 mm sand, ρ is the air density, g is acceleration of gravity, and u^*_t is the threshold friction velocity. There is a good agreement between the calculated q with the maximum observed values of Ferreira & Oliveira (2008). The authors followed the modification of the free surface due to wind erosion with time and found that the release of particles from inside the box occurs mainly at the leading edge. In the present research, this was avoided by having no sharp edges near the test surface in order to approach a flat bed situation. In addition, in place of a well defined particulate sample in terms of grain sizes, the mass loss rate for real materials

at different wind velocities was measured. The same group had previously studied the problem of coal dust release from rail wagons during transportation using a 1/25 scale model with a locomotive and four wagons placed into the wind tunnel using an undisturbed wind velocity of 13.4 m/s (Ferreira & Vaz, 2004). The experiments show that the use of covers reduces the amount of dust released by more than 80% compared to uncovered wagons. Most of the coal grains in the experiment have a diameter in the range 0.2 – 1.1 mm with the cut at 2 mm and the total mass loss was determined using an electronic balance. Roney & White (2006) measured the PM10 emission rates for different types of soil. The PM10 concentrations c and wind velocities were measured before and after the test track at different heights z and the total emission from the control volume was determined. Horizontal PM10 emission rates as high as 20 mg/m²/s were measured when the wind velocity extrapolated to 10 m height was 24.3 m/s. Roney & White (2006) also measured the total mass of fugitive dust using a sand trap. Typical values of 0.001- 0.0001 for the ratio of PM10 versus total removed mass were obtained. The authors also considered the vertical PM10 flux, which was derived from the gradient of the vertical concentration c according to the diffusion formula

$$F_a = -K u_t^* z \frac{dc}{dz} \tag{8}$$

This vertical PM10 flux was directly related to the horizontal flux of dust measured in the wind tunnel (Roney & White, 2006). Due to the locally restricted wind field it is expected that in present work most of the dust from the test surface is transported away in the horizontal direction. In setting-up wind tunnel studies of a scaled-down physical situation, it is important to consider the similarity principles. By obeying such principles, one can expect to grasp the information that is relevant to a real 1:1 situation. For example, Xuan & Robins (1994) studied the influence of turbulence and the complex terrain on dust emissions from a model coal pile including the subsequent dispersion and deposition. Although this is one possible approach for determining emissions, the present study does not deal with the wind field experiments on a scaled-down EET area. Emissions from a given test area at different wind velocities were measured instead. In the future, these data may be used in combination with computational fluid dynamics (CFD) wind simulation of the whole stockpile area to predict erosion potential of the whole stockpile area.

2.5 Watering

One of the simplest and effective means to reduce dusting is by adding water to the stock material. Due to the surface tension of the water, the inter-particle cohesive forces are larger and additional work is required to eject dust particles into the atmosphere. The influence of moisture on coal losses is known, Cowherd et al., (1988) have shown that a watering intensity of about 1 l/m²/h for an unpaved road surface results in an approximate control efficiency of 50%, presumably for total suspended PM and under normal wind conditions. Another study focuses on the pickup of soil by a belly scraper at a landfill site. The authors demonstrate that watering is effective in controlling PM10 emission at wind velocities of 18 m/s (Fitz & Bumiller, 2000). An increase of 4% in the moisture content in the upper layer of the soil was responsible for a reduction in PM10. The authors assume that the water penetrated to a depth of 0.02 m into a soil having a density of about 2800 kg/m³. This means

that a 90% reduction in the PM10 concentration at the sampling point was achieved with a watering rate of 6.5 l/m²/h.

3. Experimental design

The benchmark twenty-four hour measurements of dust made using filter-based gravimetric methods are costly and time consuming. The filter handling involves a large number of steps including pre-conditioning, weighing of blanks, filter installation and filter removal on the sampling site, post-conditioning and weighing of dustloaded filters. However, to follow up our dust emission studies time resolution of the order of at least one minute is needed.

3.1 Tapered element oscillating microbalance

The measurements of the PM10 concentrations were made using a Patashnick & Rupprecht's Series 1400a tapered element oscillating microbalance (TEOM). The most important part of the TEOM is its mass detector or microbalance, which utilizes an inertial mass weighing principle. The detector consists of a filter cartridge placed on the end of a hollow tapered tube while the other end is fixed rigidly to a base. The tube with the filter on the free end then oscillates in a clamped-free mode at its resonant frequency. This frequency depends on the physical characteristics of the tube and the mass on its free end. A particle laden air steam is drawn through the filter where the particles deposit themselves. As the amount of particulates builds up, the mass of the filter cartridge increases which decreases the frequency of the system. By accurately measuring this frequency change, the accumulated mass can be determined. In essence, the system can be considered a simple harmonic oscillator, through which the following equation can be derived,

$$\Delta m = K_0 \left(\frac{1}{f_f^2} - \frac{1}{f_i^2} \right) \tag{9}$$

where f_i and f_f are the initial and final frequency, respectively, of the system, Δm is the mass change of the system from initial value, and K_0 is the calibration (spring) constant of the tapered element. Combining the accumulated mass with the volume of air drawn through the system during sampling then yields the particle mass concentration. For ambient PM measurements the mass sensor provides a minimum mass detection limit of 0.01 μg. To avoid a problem of air humidity the air is heated typically to 50°C prior to passing through the filter. A more complete description of the instrument and conditions under which it can be used reliably is given by Patashnick & Rupprecht (1991).

3.2 Black carbon concentration by Aethalometer

As an independent device – a portable Aethalometer (Magee Scientific, AE 42-2ER-P3) was used to measure coal dust. The instrument comprised two-channels with two diode types: IR and UV. The Aethalometer provides a real-time readout of the concentration of 'Black' or 'Elemental' carbon aerosol particles ('BC' or 'EC') in an air stream and was first described by Hansen et al. (1984). Black carbon is defined by the "blackness" of an optical measurement. Physically, the Aethalometer measures attenuation of a specific wavelength of light through a quartz fibre filter as it loads over time. The 'EC' definition is based on a thermal chemical

measurement. There is no accepted definition of 'elementarily' and the different thermal parameters used by different EC analysis protocols yield different EC numerical results, even on portions of the same filter samples whereas the optical analysis for BC is consistent and reproducible (Weingartner et al., 2003). In present work the Aethalometer draws the air through the inlet port without an impactor stage. The flow rate was set to 3 l/min by a small internal pump. The dust sample is collected on a quartz fibre filter tape and photomultiplier measures the signals of diode light passing the clean exposed part of quartz filter tape, and a light beam attenuation and BC concentrations is calculated.

3.3 Auxiliary equipment

The fan is of centrifugal type 6Cv6 and produced by Klima Celje. It delivers a maximum flux of 9400 m^3/h at 3 kW. A frequency inverter Watt drive L2000 - 030HFE was additionally installed to control the power in a continuous manner. Wind velocity was measured using a wind sensor VMT 107 connected to the read-out station AMES. A hand held sensor served as a check for the wind velocity around the test area. An electronic balance My-weigh HD-150 with a capacity of 60 kg and mass resolution of 0.02 kg was employed to measure the total rate of dust emission from the test pile. The total force exerted by the effective weight of the test vessel was recorded to obtain the desired time dependence of the mass loss with good time resolution.

3.4 The wind test track

The test track was setup in the open air near to the western terminal wind barrier in order to shelter the apparatus from local wind field perturbations. Additional smaller side fences were installed to reduce the effects of any side wind. All measurements were performed during periods of stable and calm weather during June and July 2008.

The test track starts with an air stream source. The centrifugal fan produces an air stream with an adjustable air velocity through a 0.38 x 0.35 m output opening. During testing the air stream velocity at 1.30 m from the opening in the middle of the test track reached a maximum of 18 m/s and was a linear function of fan frequency, $u_{.20} = 0.352\ v - 0.398$ (v is inserted in Hz and $u_{.20}$ in m/s). The experimental wind velocities ($u_{.20}$) are referred to as the velocity measured at 0.20 m above the centre of the test vessel. On the flat plate (track), was mounted the electronic balance with the test vessel secured on the top. The vessel's dimensions are 0.60 x 0.60 m, and to reduce wind turbulence the edges were angled at 45° so that the surface of material exposed to wind erosion was 0.46 x 0.46 m. An additional wind screen was fixed on the track to reduce the effect of buoyancy on the mass measurement. The test vessel was then filled with the test material and the material levelled to the upper edge of the vessel; the layer of material in the vessel was approximately 7 cm thick. At the end of the test track was positioned the TEOM PM10 and the Aethalometer with the inlets placed 1.30 m after the vessel. The measurement consisted of submitting the vessel and test material, to airflows of different wind velocities. Each test at each velocity lasted for 10 minutes and the mass of the test vessel was recorded every 2 seconds. Every 10 seconds the PM10 concentration was recorded (10 s average composed of 5 readings) and every minute the black carbon (IR and UV) concentration. The wind speed sensor was placed behind the inlets to monitor wind speed stability.

3.5 Sample preparation

The coal and iron ore samples were separated into four and three size fractions, respectively, while hydrated alumina, which has a narrow grain size distribution, was taken directly from the cargo. 40.3 kg of the test coal, named ABK, which originates from Indonesia, was taken from the pile and fractionated as follows:

- Fraction 1 (FR 1): grain size larger than 15 mm, 27.1% of the total mass,
- Fraction 2 (FR 2): grain size between 5 and 15 mm, 25.8 % of total mass,
- Fraction 3 (FR 3): grain size between 3 and 5 mm, 9.1 % of the total mass,
- Fraction 4 (FR 4): grain size less than 3 mm, 38.0% of total mass of the coal sample.

The majority of the coal with density of 1100 kg/m^3 in the pile was present in the finest, the FR4 fraction.

The particle size distribution (relative number N of particles as a function of coal particle diameter d) of FR4 coal fraction was estimated by the following simple method. The particles were allowed to disperse according to size by dropping them through a horizontally directed stable air stream with a restricted cross section on to a horizontal metal plate. An average diameter of particles, d_i, deposited along the metal plate in each bin was determined by optical microscopy and the mass m_i of the deposit in each bin was measured accurately using a microbalance. In the log-log plot the N(d) is approximately a linear function of d suggesting that N is proportional to $d^{-1.6}$. The median diameter of the particle distribution, defined as the diameter that "splits" the number of particles into two halves, was d_{50}=40 μm. Prior to making tests on the wind test track, a maximum cone angle for three of the finest coal fractions was measured. This was achieved by building up a cone on a flat surface until the angle at the top assumed the largest value. As the angle increases, the component of the weight force acting on a coal particle along the cone surface is increased. When this force becomes larger than the friction force, exerted by the surrounding particles, the particle will start to move downhill. This is important for estimating the threshold friction velocity on inclined surfaces. Obviously, the component of the weight force "helps" the wind to lift the particles if this is blowing downhill and vice-versa.

	FR4	FR3	FR2
Base diameter (cm)	20	20	20
Height (cm)	13.0	15.5	18.0
Angle	33.0°	37.8°	42.0°

Table 2. Top cone half-angle α_t for different coal fractions.

The iron ore with 5000 kg/m^3 density was separated into three fractions:

- FR 1: d > 7 mm, 25.5 % of the total mass,
- FR 2: 3 mm < d < 7 mm, 29.2 % of the total mass,
- FR 3: d < 3 mm, 45.2 % of the total mass.

4. Results and discussion

4.1 Coal

For FR1 coal fraction no mass loss larger than 0.02 kg and no increase in PM10 or the BC signal for test wind velocities up to 18 m/s were detected during a time interval of 10 minutes and for an initial coal mass of 9 kg.

4.1.1 FR2 coal

The average background concentration of PM10 during the FR2 measurement was 73 μg/m^3 but this did not correlate with the detected mass loss. The latter was detected only at the highest wind speeds i.e. > 45 Hz (16 m/s). The Aethalometer signal was also stable during the measurements, displaying average values of 1470 ng/m^3 and 1320 ng/m^3 for the IR and UV diode, respectively. The effect of buoyancy is to make the test vessel effectively lighter when the air stream is on and is larger for higher air velocities. This results in an offset of the mass signal and can be easily accounted for in the data analysis.

4.1.2 FR3 coal

For FR3, a mass loss on a time-scale of a few minutes at a wind speed of $u_{.20}$=13.5 m/s (40 Hz) is observed (Figure 1). The effect of 18 m/s wind velocity was such as to remove approx. 20% of the material from FR3 from the vessel in 10 minutes.

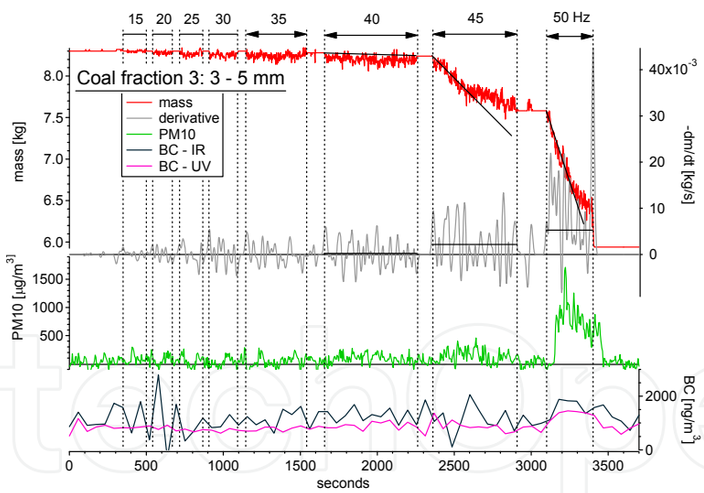

Fig. 1. Fraction 3 (FR3) measurement with a dry coal reporting the total mass (red, kg), the negative of its time derivative (gray, kg/s), PM10 concentration (green, μg/m^3), BC-IR (black) and BC-UV (pink) concentrations (ng/m^3) as a function of time. Narrow intervals between vertical dashed lines correspond to wind velocity zero. For the intervals between, the wind velocity is denoted by a frequency of the converter v depending on $u_{.20}$ in a linear fashion as presented in Section 3.4.

The results also show a correlation between the increasing PM10 concentration and the negative time derivative of the mass (-dm/dt), which is not so prominent in the BC detection channel. In fact, there should be no PM10 signal since, in principle, FR3 should not

contain particles with a diameter smaller than 3 mm. There are two possible reasons for the nonzero PM10 signal. The first is that the sieving efficiency was not 100% and some residual FR4 remained in FR3 and second, which is more probable, is that small particles are produced by creep and saltation processes. As mentioned above, this is when larger particles are eroded while rolling or jumping along the surface under the force of the wind field. If the second option prevails, then an estimate of this effect can be obtained by comparing the relative ratio of PM10 to the mass time derivative signal for FR4 (see below) and FR3 measurement: it appears that these indirect processes produce about 10% of the concentration, which would be measured in a direct PM10 removal (as dominant for FR4) for the same total mass loss.

4.1.3 FR4 coal

As expected, FR4 coal fraction is most affected by wind erosion. Figure 2 shows that while at 8 Hz the surface is stable i.e., no directly detectable change of mass in 5 min, at 15 Hz (corresponding to $u_{.20}$ = 5 m/s) there is a detectable 20 g mass loss in 360 s. At 20 Hz the loss is larger: 240 g in 1050 s. Looking at the graph one clearly sees how mass loss per unit time increases with increasing wind velocity. Typically, after switching on the wind source the mass outflow is at maximum but later drops to almost zero. In these measurements, saturation is reached at 25 Hz only. This means that after 1800 s and after a 26% mass loss (2.54 kg/9.60 kg) the surface of the coal dust in the test vessel had altered in such a way that the friction velocity of the wind was smaller than the threshold velocity for all particle sizes on the exposed surface. The oscillations in the mass loss are a probable result of oscillations in the wind velocity and are affected by the different stages through which the surface morphology alters as it reaches equilibrium at saturation. At 30 Hz the measurement had not lasted long enough to reach saturation, although 44% (4.30 kg/9.70 kg) of the initial mass m_0 had been lost. At 22 Hz the much smaller relative mass loss of 3% (0.28 kg/9.54 kg) indicates that the results are not significantly affected by changes in surface morphology. It is interesting to note that the mass time derivative, the PM10 concentration and both BC concentrations correlate with time – so that if the proportionality factors would be known

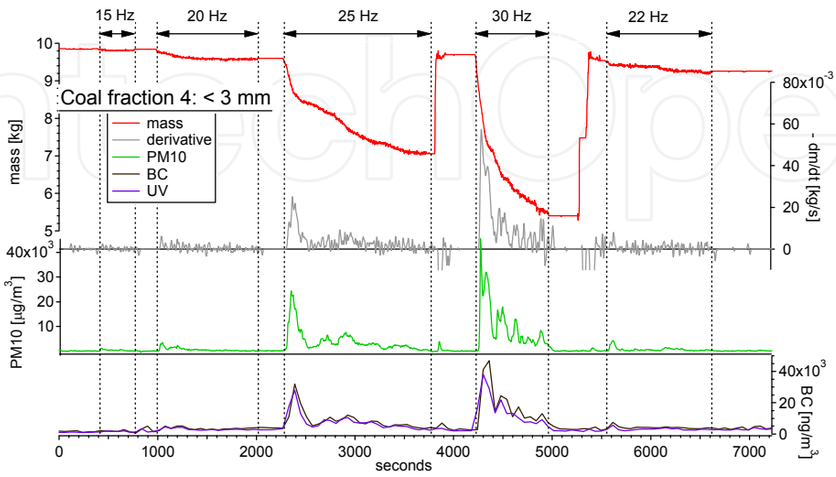

Fig. 2. The same as Figure 1 but for FR4 coal fraction.

only one of these three would suffice, since the same dynamics is observed with the three detection channels. In this case, the PM10 should be chosen for detection as it demonstrates the largest sensitivity.

4.1.4 None size-fractioning

Finally, measurements were performed on an 11 kg of dry sample of unfractionated ABK coal, taken directly from the surface of an actual pile (Figure 3). The dynamics of the mass outflow at different wind speeds reflects the dynamics of the mass outflow of the different fractions previously studied. In Figure 4, which summarizes the results for coal, the two main fraction thresholds are clearly observable, but the mass of the mixture is removed more slowly above the FR4 threshold than for the pure FR4 fraction. Instead of a rapid increase in the signal, stabilization is observed soon after the FR4 threshold; here the finer FR4 particles are being screened by the larger particles in the mixture. Alternatively, the mixture's mass is removed at a rate 3-times faster than the mass of the pure FR2 fraction but about 15 times slower than the mass of the pure FR3 fraction at equivalent wind speeds above the FR3 threshold. Below the FR3 threshold, the PM10 signal is proportional to the mass loss of the mixture, but there is relatively more PM10 component in the total mass removed than for the pure FR4 fraction: the larger particles (> 3 mm) are as efficiently removed from the mixture due to the rougher surface. However, considering the absolute concentration values and a mass weight of 38% for FR4, the PM10 signal is much smaller than in the pure FR4 case. Above the FR3 threshold, the mass outflow of the mixture is somewhere between the pure FR3 and FR2 (PM10 follows the FR3 case), while below the FR3 and above the FR4 threshold the outflow is different from zero and stable with a relatively large PM10 component.

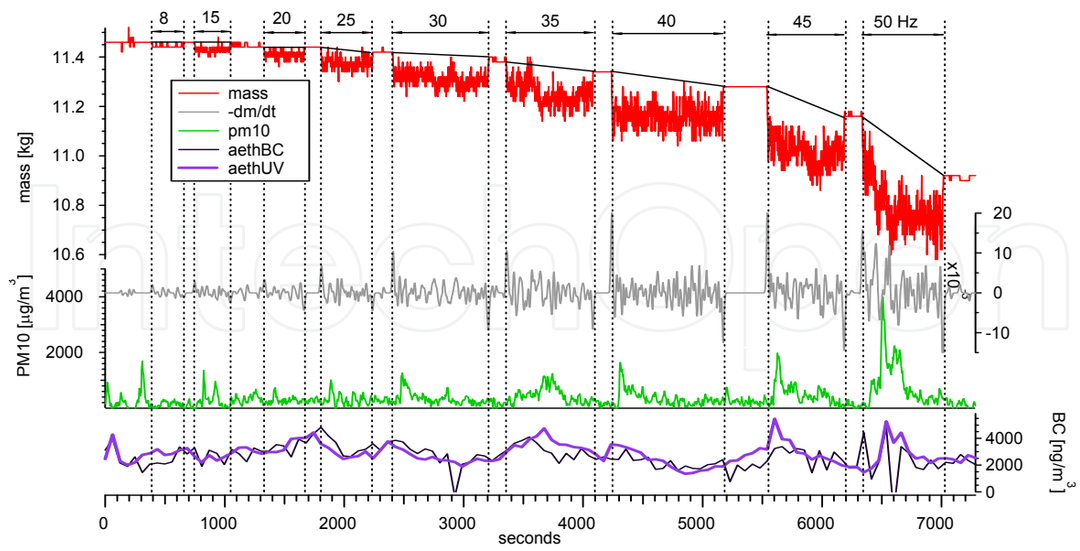

Fig. 3. The same as Figure 1 but for coal with no size-fractioning.

The threshold $u_{t.20}$ velocities for different fractions i are found by fitting the mass outflow FR_i (kg/s) with the functional form of Eq. (4) for the erosion potential:

$$FR_i = B_i (u_{.20} - u_{t.20})^2 + A_i (u_{.20} - u_{t.20}), \quad u_{.20} > u_{t.20},$$
$$FR_i = 0, \quad u_{.20} \le u_{t.20} \tag{4}$$

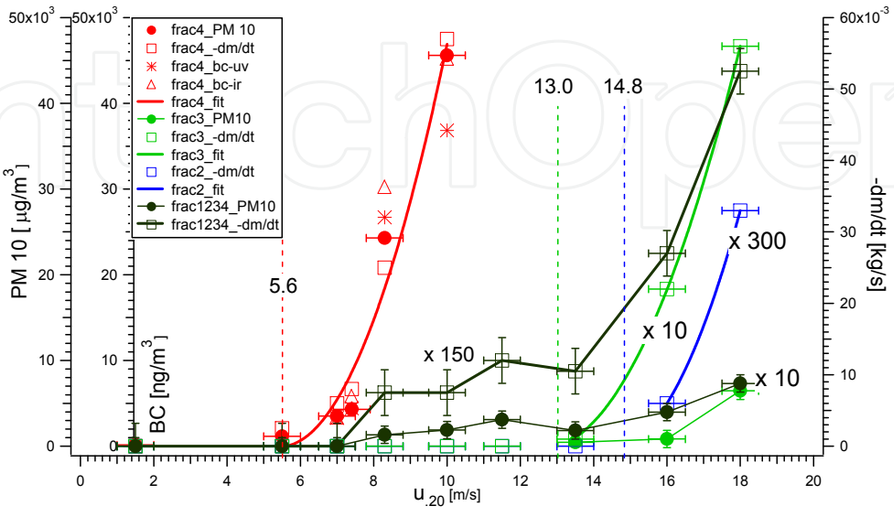

Fig. 4. The mass outflow, PM10 and BC concentrations from a 0.21 m² "unit" surface for FR2 (blue), FR3 (green), FR4 (red) and FR1234 (black) as a function of the measured wind velocity $u_{.20}$. Dashed vertical lines denote threshold velocities $u_{t.20}$ for different coal fractions.

	A_i[10^{-5} kg/m]	B_i[10^{-5} kg s/m²]	$u_{t.20}$[m/s]
FR_2	0.6	0.9	14.8
FR_3	14	19	13.0
FR_4	84	270	5.6

Table 3. Parameter values to fit the measured mass outflow.

A comparison between the observed mass losses as a function of time for different fractions of coal reveals a similar development in surface profiles with time as that reported for sand by Ferreira & Oliveira (2008), whereas Eq. (7), which was successful when dealing with sand, greatly underestimates the measured values for coal.

4.2 Iron ore

The setting-up of the test track for iron ore and alumina measurements was similar to that for coal. The test surface area was 0.35 x 0.51 m² and only mass loss was recorded. As expected from the density ratio, the iron ore is a less intensive source of dust than coal. For FR1 there was no mass loss detected up to and including $u_{.20}$ = 18 m/s.

4.2.1 Iron ore fraction 2 and 3

For FR2, the detected loss is not statistically significant. For FR3 a none zero mass loss was observed only for the largest values of $u_{.20}$, at 16 m/s and 20 m/s (Figure 5-left).

Measurements therefore show that threshold velocity $u_{t.20}$ for FR2 must be larger than 18 m/s. According to the Greeley-Iversen scheme (described below) the threshold velocity $u_{t.20}$ equal to 26.7 m/s is predicted if d_{50} = 5 mm and u^*_t = 1.5 m/s. For FR3 the measured threshold wind velocity $u_{t.20}$ is 14.0 m/s (Figure 5–right). Since this is less than 18 m/s, according to the G-I scheme the FR3 aerodynamic roughness length should be less than 300 μm and consequently, d_{50} < 9 mm. This is not in contradiction with our measurements since the maximum diameter of iron ore particles in FR3 is 3 mm.

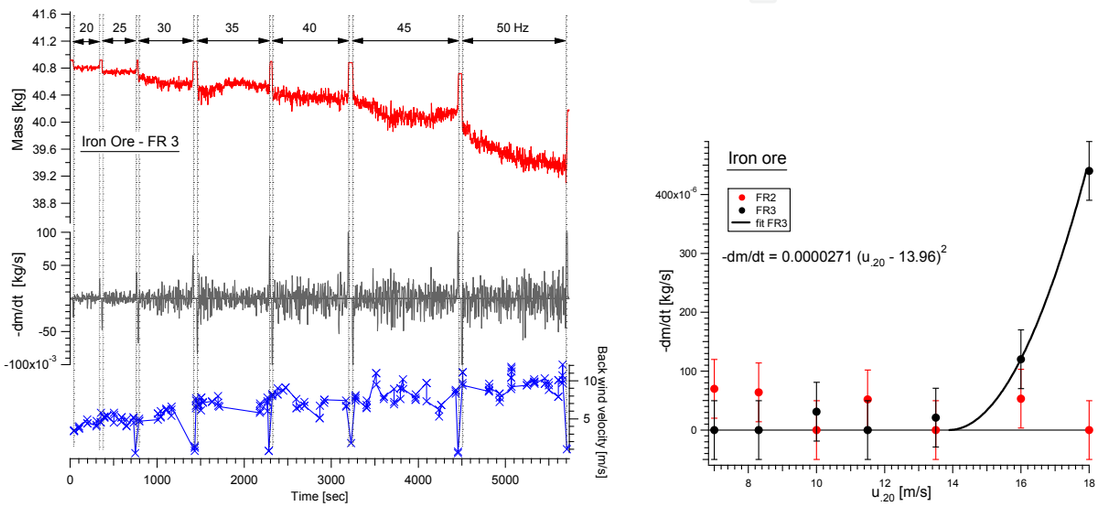

Fig. 5. -Left, FR3 iron ore mass loss measurement (red), its negative time derivative (gray) and back wind velocity (blue). -Right, the mass loss from the test surface as a function of $u_{.20}$ air velocity for FR2 (red) and FR3 (black).

4.3 Hydrated alumina

Hydrated alumina is a fine material with large erosion potential. It is usually extracted from bauxite, which is mined for the production of aluminium. In the port, the alumina is unloaded from ships using a continuous unloader and transported to silos where it is stored. Experience tells that only a small wind velocity is sufficient to lift particles of alumina into the air. Indeed, the alumina particles are small with diameters from 20-100 μm and 3200 kg/m^3 density.

The fraction of alumina tested was taken directly from the storage facility. Already at about 2.5 m/s (8 Hz) there is an observable mass loss (Figure 6 -left). It is notable that this mass loss is constant in time at any given air velocity, suggesting that no major alteration in surface morphology occurred during the test. Figure 6-right shows the results and reveals that the threshold velocity for alumina at 0.20 m above the centre of the test vessel is 2.45 m/s.

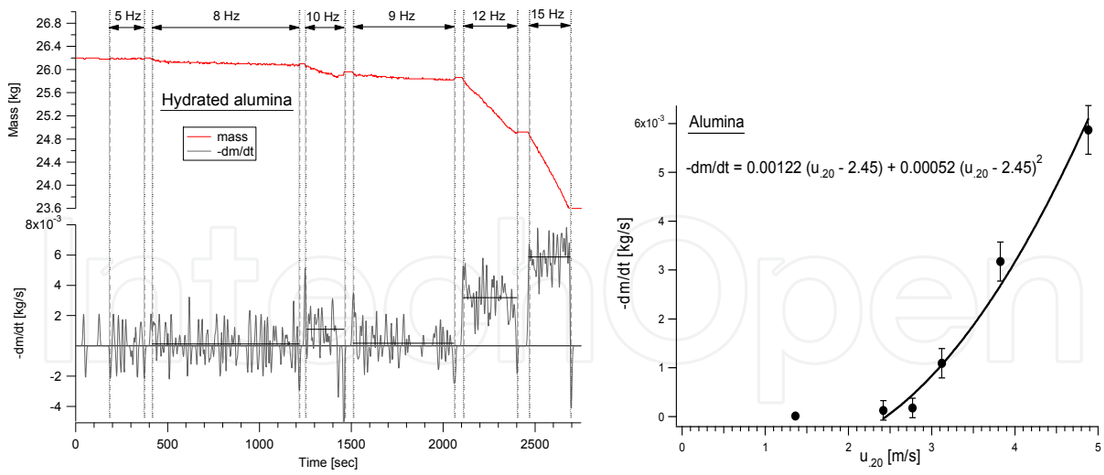

Fig. 6. -Left, the mass loss and its negative time derivative from alumina test surface with respect to time at different air velocities. -Right, the threshold wind velocity at 0.20 m above the pile is 2.45 m/s. Assuming z_0=30 μm, this gives u^*_t=0.11 m/s.

4.4 Comparison with results in the literature

Before quantifying and comparing the results for different fractions, it is important to note a few basics about the dynamics of the mass outflow. It can safely be assumed that the surface S exposed to erosion stays unchanged for a short while after the measurement begins and that the mass flux is governed by the equation dm/dt = - p S, where p is some erosion potential of the surface S. If the wind field, the shape of the surface and the composition of the surface material layer are independent of time, then the mass outflow is a constant and the mass loss will be obviously a linear function of time $m(t) = m_0 - p\,S\,t$. Such a linear drop is indeed observed in the starting time interval of each measurement. The "active" surface (affected by wind erosion) in the vessel inevitably diminishes with time and finally results in saturation (a zero mass outflow). This is reflected in the measured time dependence of the mass loss. The mass outflow diminishes with time because the wind friction velocity u^* gradually approaches (from above) the local threshold velocity u^*_t. Consistent with measurements and according to the US EPA Eq. (4), p depends quadric-linearly on the friction velocity difference $u^* - u^*_t$ but the time evolution of u^* is an unknown a priori since this is a non-local component that depends on the wind field that in turn depends on surface morphology. To predict the time dependence of the mass loss m(t) the coupled wind field - surface erosion problem must be solved. On the one hand, the erosion potential at a given point depends on the wind field, but the wind field itself depends on the erosion effect, which modifies the surface. If one is able to calculate the wind field for a particular geometry (given by function g of the coal surface z(x,y,t) in the vessel at certain time t), it is possible to estimate the alteration of the surface due to erosion for the small time interval. The wind field is then calculated again and with this knowledge a new shape of the surface is calculated, until u^* drops below u^*_t everywhere at the surface. Formally, the equations, which should be propagated in time, starting from t = 0, when the wind field is turned on, are:

$$\begin{aligned} z(x,y,t+\Delta t) &= z(x,y,t) - p(u^*(x,y,t) - u^*_t)\Delta t, \\ u^*(x,y,t+\Delta t) &= g(z(x,y,t+\Delta t)) \end{aligned} \tag{10}$$

If friction velocity u^*_t at any given time is the same everywhere along the surface (as assumed above), a reasonable assumption for a homogeneous flat terrain composed of uniform particle sizes submitted to the uniform wind field, erosion will proceed infinitely long with the same speed resulting in a constant mass outflow signal. Any reduction in the mass outflow and finally the saturation is an effect of screening, which occurs for example, when a finite quantity of material is placed in the vessel, or even for the flat terrain situation if this is composed of different particle sizes. The aim of this work was not to follow up the mass outflow with substantial modifications of surface morphology. However, for the "finite" test surface, the erosion potential p can still be measured by changing the wind velocity $u_{.20}$ above an initially flat test surface and considering only the first, linear part of the mass loss. This is true, if in this initial and relatively short period of time (so that surface morphological changes can be neglected), u^* can be thought as being frozen to a value which is the same along the whole surface area (negligible edge effects and large scale variation of u^* over the surface due to the localized wind source) and if the way that u^* is related to the measurable quantity, in our case $u_{.20}$, is known.

According to US EPA (1995), for a flat terrain with no obstacles, the wind friction velocity is related to u_{10}, the wind velocity measured at 10 m above the terrain (Eq. 1). The wind speed profile in the surface boundary layer follows a logarithmic distribution and becomes zero at the aerodynamic surface roughness height z_0 (Eq. 2). Accordingly, u^*_t is the wind speed just above the surface at $z\text{-}Z = z_0 \exp(0.4) \sim 1.5\, z_0$. Even in the case of a finite flat terrain (as in the vessel), the surface boundary behaviour is similar to that of the flat terrain if the vertical profile is limited to the region close to the surface and away from the edges. The idea is to determine the actual wind friction velocity from the simulations of the wind field for the described experimental set-up. First, the input parameters of the wind field simulation are chosen in such a way to obtain the wind velocity $u_{.20}$ value at 0.20 m above the test surface as actually measured. Then the vertical wind velocity profiles close to the surface is extracted in order to identify the region with logarithmic z/z_0 dependence and their possible differences at different parts of the surface. By comparing this local behaviour to the behaviour of the flat terrain close to the surface, the relation between the local and flat terrain situation can be established. Let it be assumed for the moment that 0.20 m is sufficiently close to the 0.46 x 0.46 m² surface so that the wind profile is defined solely by the surface characteristics, i.e. the central point 0.20 m above the surface is still in the boundary layer. As for the aerodynamic surface roughness, this is usually smaller than the particle diameter. The experimental parametrisation (Byrne, 1968) formula is

$$z_0 = Q \exp(d / \lambda) \tag{11}$$

It applies for a uniform bed of quartz particles with diameter d and parameters $Q = 2.0 \times 10^{-6}$ m and $\lambda = 6.791 \times 10^{-4}$ m. According to Eq. (11), the average d=4 mm of FR3 coal corresponds to a z_0 = 0.72 mm. If the vertical profile of the wind velocity obeys the large flat terrain law (Eq. 1 and 2) and $z - Z \approx z$, then the relation between the measured $u_{.20}$ and wind friction velocity for FR3 is given by

$$u^* = \frac{K u_{.20}}{\ln(286)} \approx 0.070\, u_{.20} \tag{12}$$

Since at threshold the wind friction velocity u^* equals the threshold velocity, the threshold velocity for FR3 coal would be, according to the measured $u_{t.20}$, approximately $u^*_t \approx 0.91$ m/s. Alternatively, for a bed composed of several grain sizes the overall roughness length is given as $z_0=d_{50}/30$ (Chane Kon et al., 2007 and references therein). For FR4 coal this means that approximately 50% of the FR4 volume is made up of particles with a diameter smaller than 1 mm so that the majority of particles have much a smaller diameter than this. Taking $d_{50} \sim 40$ µm, it comes out that $z_0 \sim 1$ µm for FR4 so that

$$u^* = \frac{K u_{.20}}{\ln(200\,000)} \approx 0.034\, u_{.20} \tag{13}$$

and consequently $u^*_t = 0.18$ m/s for FR4. This result is not greatly affected by the choice of z_0. If a 50 times larger z_0 is selected, u^*_t would increase to 0.27 m/s. Prior to any corrections due to the local wind field situation this simple scheme produces results similar to those reported by Barrett & Upton (1988). They investigated the erodibility of industrial materials in a wind tunnel. For a coal with a density of 1300 kg/m^3 and a median particle diameter of 1.67 mm the threshold value of wind friction velocity was 0.35 m/s. After removing those particles with a diameter larger than 1 mm, the friction velocity reduced to 0.22 m/s. This second measurement is a good match to FR4 estimates found in this research, while FR3 deals with larger coal particles. A large difference in the threshold velocity for FR3, i.e., 0.91 m/s versus 0.34 m/s can be to some extent explained by the difference in the aerodynamic roughness lengths. Indeed, in this case Eq. (11) needs to be extrapolated outside of actually measured range of diameters. At the upper edge of the studied interval is a particle diameter of 2.5 mm which results, according to Eq. (11), in an aerodynamic roughness length of $z_0 = 0.08$ mm. The error introduced by extrapolation to diameters greater than 2.5 mm is not known. Alternatively, although FR3 is a relatively well-defined fraction regarding particle diameter distribution, it is still composed of different grain sizes. Employing median diameter $d_{50} = 3$ mm one arives at $z_0 = 0.1$ mm. Taking this as a more realistic value, the threshold velocity for FR3 calculated by Eq. (12) is reduced to $u^*_t = 0.68$ m/s. Finally, assuming that $d_{50} = 10$ mm for FR2 (5-15 mm), the aerodynamic roughness length becomes $z_0 = 0.33$ mm so that corresponding $u^*_t = 0.94$ m/s for a measured threshold velocity $u_{t.20}$ equal to 15 m/s.

4.5 Greeley-Iversen scheme

The measured threshold velocities published by Barrett & Upton (1988) fit well into the so-called semi empirical Greeley-Iversen scheme (Greeley & Iversen 1985) that considers all physical forces acting upon a particle exposed to the wind. Chane Kon et al. (2007) gave a brief description of the scheme. Here the scheme is used to estimate the threshold friction velocity $u^*_t(d)$ for particles with diameters up to 10 mm and for materials investigated. In short, at each d the minimum of the expression

$$u^*_t(d) = A(R(u^*,d))\,F(R(u^*,d))\cdot\sqrt{1+\frac{1.9\cdot10^{-10}}{\rho_a g d^{2.5}}}\sqrt{\frac{g d(\rho_p-\rho_a)}{\rho_a}} \tag{14}$$

is sought by changing the friction velocity u^*. This enters the Reynolds number $R=u^*d/\nu$, where the kinematic viscosity of air $\nu=1.57 \times 10^{-5}$ m^2/s. The empirical functions A and F in Eq. (14) are given by

$$0.03 \le R < 0.3 : A=0.20,\ F=(1\text{-}2.5\ R)^{-0.5},$$

$$0.3 \le R < 10 : A=0.13,\ F=(1.9828\ R^{0.092} - 1)^{-0.5}, \quad (15)$$

$$10 \le R : A=0.12,\ F=1\text{-}0.0858\ \exp(-0.0617(R\text{-}10))$$

The air density ρ_a =1.24 kg/m^3 and ρ_p is the particle density. Under the first square root in Eq. (14) the diameter d must be inserted in meters. The results for coal show a good match with the scheme predictions for FR3. Obviously, the extrapolation of Eq. (11) for aerosol roughness length with d=4 mm does not lead to the right result for FR3 coal. A reasonable agreement of the Greeley-Iversen (G-I) estimate of u^*_t with the measured value is obtained also for FR2. Alternatively, FR4 has a broad particle diameter size distribution, while the G-I scheme applies to pure size fractions. Nevertheless, the measured value of 0.21 m/s is inside the velocity range 0.09 - 0.50 m/s suggested by G-I scheme. While for pure fractions the G-I scheme reliably predicts the threshold friction velocities, in the case of mixtures such as FR4 fraction of coal and FR3 fraction of iron ore it gives only a rough estimate.

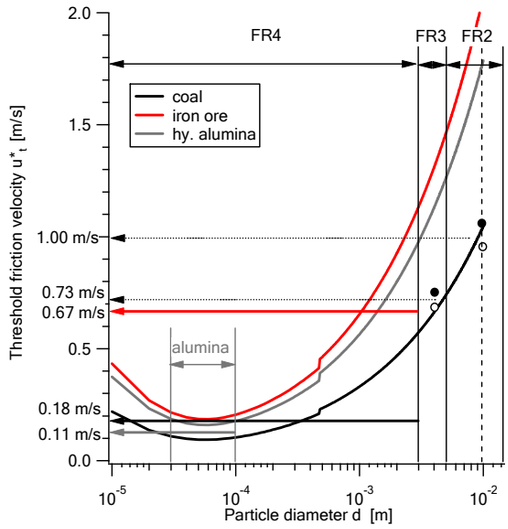

Fig. 7. Curves denote threshold friction velocity with respect to particle diameter for coal (black), iron ore (black) and hydrated alumina (gray) according to the Greeley-Iversen scheme. Hollow circles denote measured threshold friction velocities, deduced from the measured wind speed at 0.20 m above the pile centre using estimated aerodynamic roughness lengths for different fractions and materials. Full circles represent the corresponding wind field corrected data. Vertical lines mark particle diameter ranges for different materials and horizontal arrows the corresponding threshold friction velocities.

4.6 Geometric wind correction

The equations quoted above apply to flat terrain with no obstacles and a vertical wind profile independent of the base position. Because measurements were made in a restricted geometry and with a localised wind source it is important to estimate the effect that this particular set-up may have on the threshold friction velocities extracted from measured $u_{.20}$ dependence using the ”flat terrain” equations.

Two-dimensional wind simulation of the set-up does not take into account surface roughness effects. This does not seriously affect the wind field except close to the surface, in the so-called surface layer. The CFD simulation by Fluent 6.2 shows, that because of the pile, the wind velocity at 0.20 m above the pile centre has increased to 13 m/s compared to the value of 10 m/s at the same height above the flat terrain before the pile. While both profiles in the boundary layer: the "pile" and the "flat", fit well the functional form of Eq. (2), the flat profile surpasses the logarithmic extrapolation outside the boundary layer and the "pile" profile undershoots the logarithmic extrapolation. The extrapolation of fit from the boundary layer suggests the value of the wind velocity at 0.20 m above the base in the absence of geometrical and wind source constraints. According to this procedure, a measured 13 m/s wind velocity at 0.20 m above the pile is equivalent to a velocity of 14.6 m/s in a flat terrain situation. This translation is important since formulas quoted previously apply for the flat terrain situation. This simulation suggests that the measured $u_{.20}$ should be increased by a factor of 1.12 and this corrected value then used to determine the wind friction velocity. In conclusion, a particular geometry of the set-up does not affect more than 10% the threshold velocity values in the sense that these can be related to a wind velocity $u_{.20,}$ measured at 0.20 m above the centre of the test surface using just the flat terrain formulae. So, when $u_{.20}$ velocity distributions for any pile, modelled smoothly at a 0.5 m length are given, the experimental $u_{.20}$ data presented in Figure 4 can be used to estimate the total mass outflow and the corresponding PM10 and BC concentrations. Table 3 summarises our results for dry materials.

	d_{50} (mm)	z_0 (mm)	$u_{t.20}$ (m/s)	u^*_t (m/s)	u^+_{t10} (m/s)
FR2 coal	10	0.33	14.8	0.93	23.8
FR3 coal	3	0.10	13.0	0.68	19.7
FR4 coal	0.04	0.0014	5.6	0.18	7.4
FR1234 coal		0.1	5.6, 13.0		7.6, 19.7
FR2 iron		>0.3	>18		
FR3 iron		0.05	14.0	0.67	20.6
Alumina		0.03	2.5	0.11	3.6

Table 3. Threshold wind velocities $u_{t.20}$ for different fractions of coal, iron ore and alumina as determined by our measurements. Also reported are u^*_t and u^+_{t10} threshold velocities which are calculated from measured $u_{t.20}$ by using the estimates for d_{50} (z_0).

4.7 FR4 coal watering

Dusting from the coal stockpile can be significantly reduced by spraying the surface with water. The water effectively increases the mass of the particles by binding the particles to the surface layer of the coal. However, the protection afforded by a single spraying is not permanent because the water evaporates.

We measured that watering of FR4 coal by 0.5 l/m² every two hours is sufficient to suppress dusting at $u_{.20}$ = 8.3 m/s and at 95% air humidity. Compared to a dry FR4, after 364 seconds more than 100 times less mass was removed from the test vessel (1.16 kg versus 0.01 kg). To achieve the same effect at $u_{.20}$ = 11.3 m/s, 2 l/m² would be required. The estimates of a water quantity needed to suppress the dusting from FR4 surface should be considered as upper estimates when applied to realistic surface FR1234. The results are consistent with the

belly scraper case at a landfill described by Fitz & Bumiller (2000) and with the unpaved road surface watering efficiency determined by Cowherd et al. (1988). On the other hand, it is difficult to compare this study's results with those of Nicol & Smitham (1990), because neither exposure time nor wind velocity is reported. While they made wind tunnel tests with uniformly humid and conditioned coal, in our case the water was sprayed directly onto a dry coal surface just prior to switching on the air stream. Measurements show that mass loss is not a steady function of time, except when the watering is sufficient to establish a lasting linear dependence of mass loss with time. For the two linear cases with $u_{.20}$ equal to 8.3 m/s and 11.3 m/s the mass losses for the coal (+ water) system were 480 g/m²/h and 1400 g/m²/h, respectively. In both cases water evaporation contributed mostly to the mass loss, as shown by a separate wind track experiment with water sample only.

4.8 Iron ore watering

Concerning iron ore, the following phenomenon was observed: after watering, the surface of the iron ore (FR4, FR3) developed a firm crust upon drying. The formation of the crust strongly reduces the dusting potential and a much lower mass loss per unit time is observed for crusted material than for freshly sieved iron ore under the same experimental conditions. Only 0.06 kg loss in 1548 seconds was observed for the crusted FR3 iron ore at $u_{.20}$=18 m/s, which is 9-times less than for sieved FR3. In view of this finding, it is highly desirable to crust the iron ore, which is stored for a significant period. Different to the coal, watering the iron ore only once is sufficient to immobilize it, provided the crust remains intact and is not disrupted by subsequent movement of heavy machinery.

The mechanism behind the hardening of iron ore is attributed to agglomeration of iron ore particles. PIXE analysis, as well as x-ray diffraction of an iron ore sample shows that the ore consists of 98% pure hematite (Fe_2O_3) with small impurities of K, Ca, Cl, Ti, Mn and Sr. According to specifications, other impurities may be mixed with the ore in small quantities (SiO_2 < 3%, Al_2O_3 ≈ 1%), but in this authors opinion it is the content of water which is responsible for binding. When hematite is watered and left to dry a uniform crust develops over the sample. The crust can be destroyed by mechanical action or by re-watering the iron ore. As found out previously, the first two water layers near the hematite surface are highly ordered, and effectively are adsorbed to the surface through hydrogen bonding and further from the surface, water still displays some ordering in the form of layering (Catalano et al., 2009). Different hematite particles are bound between themselves by the interaction of these water layers, which are not removed in the process of drying. Upon heating an iron ore sample to 600 °C the water is completely removed and the mass percentage of this "residual" water is about 1%. No such effect is observed for coal. Upon drying, the chemical structure of iron ore is not changed, as shown by x-ray diffraction measurements.

5. Conclusions

Time dependence of mass loss from the test surface was measured together with concentrations of inhalable particulate matter (PM10) and black carbon (BC) in the vicinity of the test surface for wind velocities ranging from 1 - 18 m/s at 0.20 m above the centre of the test surface. Threshold wind velocities $u_{t.20}$ were measured for four different size fractions of coal and for three different fractions of iron ore stored at the terminal, and for hydrated alumina - a strong dust emitter. The same set up was employed to study the

suppression of dust emitted by the finest coal fraction (d < 3 mm) upon watering of the dry test surface. By CFD modelling the similarity of our size limited test track was examined with respect to a flat terrain situation. The analysis shows that measured wind velocity thresholds for different fractions are consistent with the predictions of the Greley-Iversen scheme. Although the dusting potential of the non-fractioned (realistic) coal sample reflects dusting potentials of its fractions, measurements show that the former cannot be estimated simply by a weighted average of different fractions. Watering (1.0 l/m²/h) of the coal surface reduced the mass outflow by one hundred times with respect to the dry coal surface when $u_{.20}$ = 11.3 m/s. Alternatively, stabilisation of the iron ore surface can be achieved by a single act of watering; upon drying agglomeration of hematite particles occurs and a firm crust forms on the surface strongly reducing further dusting.

Although CFD calculations of a large real scale physical configuration are necessary to obtain the final result concerning emissions (Loredo-Souza et al., 2004; Torano et al., 2007; Diego et al., 2008), the precise measurements of the "dusting" potential generated by the "unit" test surface under different conditions are important as they provide relevant input parameters for the simulation. To demonstrate further the use of the results, the measured erosion potential is employed to estimate the PM10 emission from a real stockpile in a single disturbance.

In Port of Koper the open air (EET) coal terminal stores approximately 660000 m³ of coal. If the height of the pile is 8 m and the top cone angle is about 40°, the surface area covered by the pile is about 100000 m². Based on the data obtained, and prior to any CFD simulations it is possible to roughly estimate the intensity of dusting from the EET if several simplifying assumptions are invoked. First, we neglect the effect of the fence which actually surrounds the pile, as well as any deviations from the flat terrain situation, i.e the pile edges. Then, according to the experimental data for FR1234, the dry coal pile does not emit PM10 particles until $u_{.20}$ < 5 m/s. For wind velocities 5 m/s < $u_{.20}$ < 18 m/s the ten-minute average PM10 concentration, denoted by $\langle c \rangle$ is found to increase from 100 µg/m³ at the lower limit to 700 µg/m³ at the higher velocity limit. To maintain the average concentration for t = 10 minutes in the rectangular box with a cross section of s = 0.4 x 0.4 m² and length of $l=u_{.20}\,t$ the test surface released $\langle c \rangle\, s\, t\, u_{.20}$ mass of the PM10 coal particles. This means that the test unit surface of 0.21 m² in 10 minutes releases from 0.048 g (at $u_{.20}$ = 5m/s) to 1.2 g (at $u_{.20}$ = 18 m/s) of PM10. The whole (and dry) coal stockpile at ETT would then release 22 kg to 570 kg of PM10 matter in 10 minutes. The source strength of PM10 emission is not constant but diminishes with time (see for example Figure 2); after 10 minutes it becomes small compared to the source strength at the beginning, i.e., when the air stream is just switched on. The US EPA Eq. (4) employs a concept of a number of disturbances per year: the duration of disturbance is unimportant; it is just the highest wind velocity that determines the quantity of dust emitted in a single disturbance. In fact, what is described above is just a 10 minutes long disturbance and it is interesting to see, how the US EPA estimate correlates with our.

To generate an EPA estimate it is important to express the difference between the friction velocity and the threshold friction velocity. Assuming that the roughness height z_0 is known, both threshold velocities can be expressed by the corresponding velocities at 0.20 m above the surface:

$$u^* - u_t^* = K / \ln[0.20 / z_0](u_{.20} - u_{.20}^*) \tag{16}$$

In an extreme case when $u_{.20}$ = 18 m/s (u^{+}_{10} = 27.2 m/s, assuming z_0 = 0.0001 m) and the threshold velocity value (FR3) of $u_{t.20}$ = 13.0 m/s, EPA Eq. 3 gives 5.3 g/m² of PM10, which translates to 530 kg of material removed from the real stockpile by a single disturbance. This result matches very closely our estimate of 570 kg.

The lifted material is carried away by the wind and dispersed into the atmosphere. The PM10 concentration around the pile depends on the exact location. A detailed compilation of the PM10 concentration 3D distribution can be derived from knowing the actual wind field around the real stockpile area, which CFD simulation can provide. There is an important caveat, within the measured PM10 emission strengths it is not possible to distinguish between PM10 particles that are lifted directly by the force of the wind (suspension) and those emitted due to the saltation of heavier and larger particles along the surface. It is believed that the majority of the PM10 material is emitted due to the latter processes since the cohesion forces between the finest particles are too strong to allow direct wind entrainment (Shao et al., 1993). At sufficiently high wind speeds these large particles enter the neighbouring unit surfaces on the pile, effectively increasing PM10 emission strength of the neighbouring unit's surfaces with respect to the "parent" or "self" test surface contribution. In fact, as seen for FR1234, the mass lost into PM10 is more than one hundred times lower than the total mass, which "vanished" from the test surface by moving to the neighboring area. Most of this mass may contribute to PM10 emissions from the neighbouring surfaces. This saltation process, in fact, seems to be the origin of the nonzero PM10 emission in the case of FR3 coal (Figure 1), while in the case of FR4 and FR1234 the creeping and saltating particles which form the total "missing" mass, generate a major part of observed PM10 concentration. In this sense, the single-unit-surface PM10 emission strengths are the lowest estimates. However, for FR1234 the saltating particles are expected not to propagate far from the parent unit since the surface is relatively rough – this is required by another assumption that the stockpile keeps its shape under the force of wind.

A comment is necessary about particle removal efficiency on slanted surfaces. We saw that on an inclined surface particles are effectively lighter, if the wind blows downhill and vice versa, they are more difficult to remove when the wind blows uphill. When the top cone half-angle is at the threshold value α_t (Table 2) the particles move downhill by themselves even when wind friction velocity is zero. The crudest approximation is obtained by linearization: if the threshold velocity for downhill wind direction is zero, for an uphill wind direction it is twice the value which applies to a flat surface. The threshold velocity for particles on a "critically" slanted surface can be therefore approximated by

$$u_{.20}(\varphi) = u_{.20} + u_{.20}(2\varphi / \pi - 1) \tag{17}$$

where φ is an angle between the wind direction and local downhill direction in the plane of the inclined surface. If the inclination is less than critical, i.e. the top cone half-angle α is larger than threshold angle α_t, $u_{.20}(\varphi)$ deviates less from the $u_{.20}$ of the flat horizontal terrain because in this case an additional factor ($\cos\alpha/\cos\alpha_t$) multiplies second term on the left of Eq. (17). A more accurate description of slanted situation could be obtained by rederiving the G-I scheme. However, due to other deficiencies of the scheme (it applies for pure size fractions), the above correction may be accurate enough for samples with mixed size fractions.

Finally, it is interesting to estimate how much of the mass in total is removed by the action of the wind. From Figure 5 it can be seen that the FR1234 mass loss increases from 0.5 g/s/m² to 2.5 g/s/m² when the wind speed $u_{.20}$ increases from 5 m/s to 18 m/s. In 10 minutes, the total mass displaced over the flat surface of the pile would be 30 to 150 tonnes respectively. At the same time this action would generate at least 22 kg and 570 kg of PM10 dust, respectively.

6. Acknowledgment

We gratefully acknowledge the support of Jožef Stefan International Postgraduate School and of Environmental Agency of the Republic of Slovenia (ARSO).

7. References

Andrae, M. O. (2001). The dark side of aerosols, *Nature,* Vol.409, pp. 671-672

Archer, V. E. (1988). Lung cancer risks of underground miners: cohort and case-control studies, *Yale Journal of Biology and Medicine,* Vol.61, pp. 183–193

Bagnold, R. A. (1941). The Physics of Blown Sands and Desert Dunes, ISBN 0-486-43931-3 (Mineola: Dover Publications 2005).

Barrett, C. F. & Upton S. L. (1988). Erodibility of stockpiled materials – a wind tunnel study, *Report no.* LR 656 (PA) M, Warren Spring Laboratory: Stevenage, UK

Borrego, C; Costa, A. M.; Amorim, J. H.; Santos, P.; Sardo, J.; Lopes, M. & Miranda, A.I. (2007). Air quality impact due to scrap-metal handling on a sea port: A wind tunnel experiment, *Atmospheric Environment,* Vol.41, pp. 6396-6405

Boyd, J. T.; Doll, R.; Faulds, J. S. & Leiper, J. (1970). Cancer of the lung in iron ore (haematite) miners, *British Journal of Industrial Medicine*, Vol.27, pp. 97-105

Byrne, R. J. (1968). Aerodynamic roughness criteria in aeolian sand transport, *Journal of Geophysical Research,* Vol.73, pp. 541-547

Catalano, J. G.; Fenter, P. & Park, C. (2009). Water ordering and surface relaxations at the hematite (110) – water interface, *Geochimica and Cosmochimica Acta,* Vol.73, pp. 2242-2251

Chakraborty, M. K.; Ahmad, M.; Singh, R. S.; Pal, D.; Bandopadhyay, C. & Chaulya, S. K. (2002). Determination of the emission rate from various opencast mining operations, *Environmental Modelling & Software,* Vol.17, pp. 467–480

Chane Kon, L.; Durucan, S. & Korre A. (2007). The development and application of a wind erosion model for the assessment of fugitive dust emissions from mine tailings dumps, *International Journal of Mining, Reclamation & Environment,* Vol.21(3), Taylor & Francis, pp. 198–218

Cowherd, C.; Muleski, G. E. & Kinsey, J.S. (1988). Control of Open Fugitive Dust Sources; EPA-450/3-88/008; *Prepared by Midwest Research Institute*, Kansas City, MO, for Office of Air Quality Planning and Standards, U.S. Environmental Protection Agency: Research Triangle Park, NC

Diego, I.; Pelegry, A.; Torno, S.; Torano, J. & Menendez, M. (2008). Simultaneous CFD evaluation of wind flow and dust emission in open storage piles, *Applied Mathematical Modelling,* Vol.33, pp. 3197-3207

Ferrari, L. M.; Pender, E. & Lundy, R. (1986). Dust control on coal haul roads, *Institution of Engineers Australia*, Workshop on coal fugitive dust control of coal industry works, pp. 19-26.

Ferreira, A. D. & Olivieira, R. A., (2008). Wind erosion of sand placed inside a rectangular box, *Journal of Wind Engineering and Industrial Aerodynamics*, Vol.97, pp. 1-10

Ferreira, A. D. & Vaz, P. A. (2004). Wind tunnel study of coal dust release from train wagons, *Journal of Wind Engineering and Industrial Aerodynamics,* Vol.92, pp. 565-577

Fitz, D. R. & Bumiller, K. (2000). Evaluation of Watering to Control Dust in High Winds, *Journal of the Air & Waste Management Association,* Vol.50, pp. 570-577

Gillette, D.A. (1977). Fine particulate emissions due to wind erosion. *Transactions of the American Society of agricultural Engineers,* Vol.20, pp. 890–987

Greeley, R. & Iversen, J.D. (1985). Wind as a Geological Process on Earth, Mars, Venus and Titan, ISBN 0-521-24385-8 (*Cambridge University Press: New York*)

Hansen, A. D. A.; Rosen, H. & Novakov T. (1984). The aethalometer – an instrument for real time measurement of optical absorption by aerosol particles, *The Science of Total Environment,* Vol.38, pp. 191-196

King, E. J.; Harison, C. V.; Mohanty, G. P. & Nagelschmidt, G. (1955). The effect of various forms of alumina on the lungs of rats, *Journal of Pathology and Bacteriology,* Vol.69, pp. 81-93

Kinsey, J. S.; Linna, K. J.; Squier, W. C.; Muleski, G. E. & Cowherd, C. (2004). Characterization of the fugitive particulate emissions from construction mud/dirt carryout, *Journal of the Air & Waste Management Association,* Vol.54, pp. 1394-1404

Lawler, A. B.; Mandel, J. S.; Schuman, L. M. & Lubin J. H. (1985). A retrospective cohort mortality study of iron ore (hematite) miners in Minnesota, *Journal of Occupational Medicine,* Vol.27, pp. 507-517

Lee, S. J.; Park, K. C. & Park, C. W. (2002). Wind tunnel observations about the shelter effect of porous fence on the sand particle movements, *Atmospheric Environment,* Vol.36, pp. 1453-1463

Leon, G.; Perez, L. E.; Linares, J. C.; Hatmann, A. & Quintana M. (2007). Genotoxic effect in wild rodents (Rattus rattus and Mus musculus) in an open coal mining area, *Mutation Research,* Vol.630, pp. 42-49

Loredo-Souza, A. M. & Schettini E. B. C. (2004). Wind Tunnel Studies on the Shelter Effect of Porous Fences on Coal Piles Models of the CVRD – Vitoria, Brazil, In: *Proceedings of the A&WMA's 98th Annual Conference & Exhibition – Exploring Innovative Solutions*, Minneapolis, Minnesota, USA, June 21-24

Mohamed, A. M. O. & Bassouni K. M. E. (2006). Externalities of Fugitive Dust, *Environmental Monitoring and Assessment,* Vol.130, pp. 83-98

Nemery, B. (1990). Metal toxicity and the respiratory tract, *European Respiratory Journal,* Vol.3, pp. 202-219

Nicol, S. K. & Smitham J. B. (1990). Coal stockpile dust control*, Institution of Engineers Australia*, International coal engineering conference Sydney, pp. 154-158

Patashnick, H. & Rupprecht E. G. (1991). Continuous PM10 measurements using a tapered element oscillating microbalance, *Journal of the Air & Waste Management Association,* Vol.51, pp. 1079-1083

Parsons, D. R.; Wiggs, G.; Walker, I.; Ferguson, R. & Garvey B. (2004). Numerical modelling of airflow over an idealised traverse dune, *Environmental Modelling & Software,* Vol.19, pp. 153–162

Peralba, M. C. R. (1990). Caracterizacao quimicia dos hidrocarbonatos de betumens de carvoes sul-brasileiros, In: *Dissertacao de Doutorado, Instituto di Fisica e Quimica de Sao Carlos*, Brasil, http://hdl.handle.net/10183/28215

Roney, J. A. & White, B. R. (2006). Estimating fugitive dust emission rates using an environmental boundary layer wind tunnel, *Atmospheric Environment,* Vol.40, pp. 7668-7685

Routledge, H. C. & Ayers, J. G. (2006). Cardiovascular Effects of Particles, *Air Pollution Reviews,* Vol.3, pp. 19-42

Saxton, K.; Chandler, D.; Stetler, L.; Lamb, B.; Claiborn, C. & Lee, B. (2000). Wind Erosion and Fugitive Dust Fluxes on Agricultural Lands in the Pacific Northwest, *Transactions of the ASAE 2000*, Vol. 43(3), pp. 623-630

Shao, Y.; Raupach, M. R. & Findlater, P. A. (1993). The effect of saltation bombardement on the entrainment of dust by wind, *Journal of Geophysical Research,* Vol.98, pp. 12719–12726

Smitham, J. B. & Nicol, S. K. (1990). Physico-chemical principles controlling the emission of dust from coal stockpiles, *Powder Technology,* Vol.64, pp. 259-270

Stunder, B. J. B. & Arya, S. P. S. (1988). Windbreak effectiveness for storage pile fugitive dust control: a wind tunnel study, *Journal of Air Pollution Control Association,* Vol.38, pp. 135–143

Torano, J. A.; Rodriguez, R.; Diego, I.; Rivas, J. M. & Pelegry, A. (2007). Influence of the pile shape on wind erosion CFD emission simulation, *Applied Mathematical Modelling,* Vol.31, pp. 2487-2502

US EPA (1995). AP 42, Chapter 13: Miscellaneous Sources, (Section 13.2.1: Dusting From Unpaved And Paved Roads, Section 13.2.4: Aggregate Handling And Storage Pile, Section 13.2.5: Industrial Wind Erossion), Fifth Edition, vol.I, http://www.epa.gov/ttn/chief/ap42/ch13/index.html

US EPA (1996). Executive summary. In: Air quality criteria for particulate matter. Vol.1, Research Triangle Park, NC, U.S. Environmental Protection Agency, Natinal Center for Environmental Assessment, EPA Publication No. EPA/600/P-95/001aF, pp. 1-21

US EPA (1998). Revised Draft – User's Guide for the AMS/EPA Regulatory Model – AERMOD, Office of Air Quality Planning and Standards, Research Triangle Park, NC

Weingartner, E.; Saathoff, H.; Schnaiter, M.; Streit, N.; Bitnar B. & Baltensperger U. (2003). Absorption of light by soot particles: determination of the absorption coefficient by means of aethalometers, *Aerosol Science,* Vol.34, pp. 1445-1463

White, B. & Tsoar, H. (1998). Slope effect on saltation over a climbing sand dune, *Geomorphology,* Vol.22, pp. 159–180

Witt, P. J.; Carey, K. & Nguyen, T. (2002). Prediction of dust loss from conveyors using CFD modelling, *Applied Mathematical Modelling*, Vol.26 (2), pp. 297– 309

Xuan, J. & Robins, A. (1994). The effects of turbulence and complex terrain on dust emissions and depositions from coal stockpiles, *Atmospheric Environment,* Vol.28, pp. 1951-1960

Žitnik, M.; Jakomin, M.; Pelicon, P.; Rupnik, Z.; Simčič, J.; Budnar, M.; Grlj, N. & Marzi, B. (2005). Port of Koper – Elemental concentrations in aerosols by PIXE, *X-Ray Spectrometry,* Vol.34, pp. 330-334.

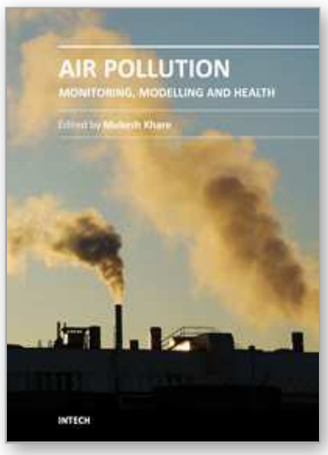

Air Pollution - Monitoring, Modelling and Health

Edited by Dr. Mukesh Khare

ISBN 978-953-51-0424-7
Hard cover, 386 pages
Publisher InTech
Published online 23, March, 2012
Published in print edition March, 2012

Air pollution has always been a trans-boundary environmental problem and a matter of global concern for past many years. High concentrations of air pollutants due to numerous anthropogenic activities influence the air quality. There are many books on this subject, but the one in front of you will probably help in filling the gaps existing in the area of air quality monitoring, modelling, exposure, health and control, and can be of great help to graduate students professionals and researchers. The book is divided in two volumes dealing with various monitoring techniques of air pollutants, their predictions and control. It also contains case studies describing the exposure and health implications of air pollutants on living biota in different countries across the globe.

How to reference

In order to correctly reference this scholarly work, feel free to copy and paste the following:

Nebojša Topić and Matjaž Žitnik (2012). Fugitive Dust Emissions from a Coal-, Iron Ore- and Hydrated Alumina Stockpile, Air Pollution - Monitoring, Modelling and Health, Dr. Mukesh Khare (Ed.), ISBN: 978-953-51-0424-7, InTech, Available from: http://www.intechopen.com/books/air-pollution-monitoring-modelling-and-health/fugitive-dust-emissions-from-a-coal-iron-ore-and-hydrated-alumina-stockpile

INTECH
open science | open minds

InTech Europe
University Campus STeP Ri
Slavka Krautzeka 83/A
51000 Rijeka, Croatia
Phone: +385 (51) 770 447
Fax: +385 (51) 686 166
www.intechopen.com

InTech China
Unit 405, Office Block, Hotel Equatorial Shanghai
No.65, Yan An Road (West), Shanghai, 200040, China
中国上海市延安西路65号上海国际贵都大饭店办公楼405单元
Phone: +86-21-62489820
Fax: +86-21-62489821

IntechOpen